Journal of Alloys and Compounds 509 (2011) 1255–1260

Contents lists available at ScienceDirect

Journal of Alloys and Compounds

journal homepage: www.elsevier.com/locate/jallcom

Microstructural evolution in laser deposited nickel–titanium–carbon in situ metal matrix composites

S. Gopagoni[a], J.Y. Hwang[a,*], A.R.P. Singh[a], B.A. Mensah[a], N. Bunce[a], J. Tiley[b], T.W. Scharf[a], R. Banerjee[a]

[a] Center for Advanced Research and Technology and Department of Materials Science and Engineering, University of North Texas, Denton, TX 76203, United States
[b] Materials and Manufacturing Directorate, Air Force Research Laboratory, Dayton, OH 45433, United States

ARTICLE INFO

Article history:
Received 16 July 2010
Received in revised form
29 September 2010
Accepted 30 September 2010
Available online 1 November 2010

Keywords:
Metal matrix composite
Laser deposition
Ni–Ti–C
Microstructural evolution
Mechanical properties

ABSTRACT

Laser deposition of a mixture of elemental nickel, titanium, and carbon (graphite) powders via the laser engineered net shaping (LENS) process results in an in situ titanium carbide reinforced nickel metal matrix composites. The composites have been characterized in detail using X-ray diffraction, scanning electron microscopy (including energy dispersive spectroscopy mapping), Auger electron spectroscopy, and transmission (including high resolution) electron microscopy. Both primary and eutectic titanium carbides, observed in this composite, exhibited the FCC-TiC structure (NaCl-type). Detailed characterization of the nickel/titanium carbide interface was carried out using high resolution TEM with the orientation relationship between the phases being ⟨1 0 0⟩ TiC//⟨1 1 0⟩ Ni and (0 0 2) TiC//($\bar{1}$ 1 1) Ni. Mechanical and tribological testing determined that the composites exhibited a relatively high hardness of 370 VHN and a steady-state friction coefficient of ~0.5, both improvements in comparison to LENS deposited pure Ni.

1. Introduction

Metal matrix composites (MMC) are used in several engineering applications including aerospace applications, due to their higher specific stiffness and strength, and, promising high temperature mechanical properties such as creep resistance [1,2]. Various metals Al, Cu, Fe, Mg, Ti, Ni, etc are used as matrices with titanium carbide as the reinforcement phase since it has high hardness (2859–3200 HV), high melting point (3067 °C), low density (4.93 g/cm^3), and high mechanical strength [3–8]. Though titanium carbide (TiC) is very hard, it is extremely brittle, and consequently is used in engineering applications more as a reinforcement in a ductile and tough metal matrix (e.g. nickel) rather than as a monolithic ceramic. Furthermore, nickel and nickel-base superalloys are employed in a wide range of applications, including aircraft jet engines, land-based turbines, and chemical/petrochemical plants. Therefore, the combination of titanium carbides reinforcing a nickel-base matrix is very promising as a hybrid material for high temperature structural applications such as automotive and aerospace applications. Recently, a study on the in situ forming methods which leads to carbide formation directly during the fabrication process has been widely used to enhance the mechanical properties in metal matrix composites [9–14]. The in situ process exhibits good interfacial bonding, thermodynamic stability, and finer particle distribution of the carbides in the metal matrix. Furthermore, the stability of these metal and ceramic interfaces is important for mechanical performance, which is critically dependent on the structural conformity of the two phases at the interface. There have been direct in situ laser fabrication processes which have successfully manufactured TiC reinforced nickel matrix composites [6,13]. However, the fabrication routes and processing mechanism of in situ laser process are not well understood.

The present paper focuses on laser deposition of metal–matrix composites based on Ni–Ti–C using the laser engineered net shaping (LENS) process. The aim is to exploit the inherent rapid solidification rate in LENS processing to achieve a homogeneous distribution of titanium carbide precipitate reinforcing the nickel matrix, while maintaining the volume fraction of these precipitates relatively low. The three salient features of the present investigation are listed below:

1. Laser deposition of Ni–TiC composites with a relatively low volume fraction of refined homogeneously distributed carbide precipitates resulting from an in situ reaction between elemental titanium and carbon (graphite) within the molten nickel pool.
2. Detailed characterization of the Ni/TiC interface using high resolution electron microscopy.
3. Evaluation of the microhardness and tribological properties of this novel in situ composite with comparisons to laser deposited pure Ni.

* Corresponding author. Tel.: +1 940 369 5353; fax: +1 940 565 4824.
E-mail address: Junyeon.Hwang@unt.edu (J.Y. Hwang).

0925-8388/$ – see front matter © 2010 Elsevier B.V. All rights reserved.
doi:10.1016/j.jallcom.2010.09.208

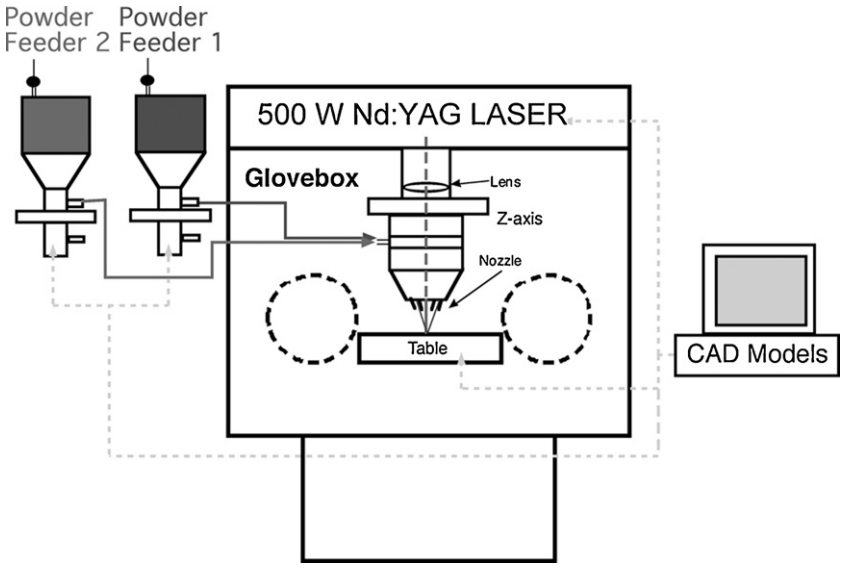

Fig. 1. Schematic representation of the laser engineered net shaping (LENS™) system.

2. Experimental

A commercial LENS™ 750 system, manufactured by Optomec Inc., was used for processing these composites. Similar to rapid prototyping technologies such as stereolithography, the LENS process begins with a computer-aided design (CAD) design file of a three-dimensional component, which is sliced into series of layers electronically. The LENS process is a direct laser fabrication processing and solid freedom fabrication process. To build three-dimensional components, the powders are injected into a focused, high power laser beam on the substrate which the deposition is occurring by consecutive layers to obtain homogeneity. The detailed mechanism of this process has been reported elsewhere [15–17]. The information about each of these layers is transmitted to the manufacturing assembly. The entire deposition is carried out inside a glove box with a controlled inert argon gas environment. The argon gas is continuously re-circulated during the LENS deposition process. A metal substrate is used as a base for depositing the component. A schematic diagram of the LENS system is shown in Fig. 1. In this case, a nickel plate substrate was used for depositing the Ni–Ti–C in situ composites. A high powered 500 W Nd:YAG laser, emitting near-infrared laser radiation at a wavelength of 1.064 μm (1064 nm), is focused on the substrate to create a melt pool into which the powder feedstock is delivered through an inert gas flowing through a multi-nozzle assembly. The nozzle is designed such that the powder streams converge at the same point on the focused laser beam. Subsequently the substrate is moved relative to the laser beam on a computer-controlled stage to deposit thin layers of controlled width and thickness [15]. The scan speed of the Nd:YAG laser was 10 in./min and the hatch width used for the deposition was 0.018 in. with 0.01 in. of layer thickness. Each layer of scan is deposited in a sequence of 0°, 90°, 180°, and 270° to ensure uniform layers. The oxygen content in the glove box was maintained below 10 ppm during all the depositions. The measured powder flow rate was 2.57 g/min while the argon volumetric flow rate was maintained at 3 l/min. The powders used for depositing the Ni–Ti–C composites consisted of commercially pure near-spherical Ni (40–150 μm) powders, pure Ti (40–150 μm) and Ni coated graphite powders (all from Crucible Research™). Prior to deposition, the nickel, titanium, and nickel coated graphite powders were pre-mixed in a twin-roller mixer. This mixing was carried out for 6 h, after which the powder was introduced into the power feeder of the LENS deposition system and the composites were laser deposited. These powders were mixed with the nominal composition 80 at%Ni–10 at%Ti–10at%C (henceforth this composition will be referred to as Ni–10Ti–10C for brevity). The composites were laser deposited in a cylindrical geometry of diameter 10 mm and height 10 mm. The laser power used in these depositions was 350 W.

The LENS deposited in situ composites were characterized by scanning electron microscopy (SEM) in a FEI Quanta ESEM. The micro-hardness was measured using a standard Vickers micro-hardness tester using 300 g load. X-ray diffraction experiment was carried out in a Rigaku Ultima III diffractometer with a Cu Kα incident X-ray source. In addition, the LENS deposited composites were also characterized by transmission electron microscopy (TEM). 3 mm diameter disc specimens were prepared using a combination of electro-discharge machining (EDM) and low-speed diamond saw sectioning. These discs were mechanically thinned using a series of abrasive papers starting from 600 grit up to 1200 grit. Subsequently, these discs were further mechanically thinned in a Gatan dimple grinder, and then ion-milled to electron transparency in a Gatan Duo Mill using 5 keV. The TEM specimens were characterized in a FEI Tecnai F20 field-emission gun (FEG) TEM at an operating voltage of 200 keV. In addition, elemental distributions of carbon, titanium and nickel were mapped by Auger electron spectroscopy with a 670xi Scanning Auger Nanoprobe operating at 20 kV and 10 nA. Sliding friction and wear testing was conducted with a Falex (Implant Sciences) ISC-200 pin-on-disk (POD) system at room temperature. The samples were openly exposed in lab air (~40% RH) during the tests. Tests were performed under a 1 N normal load with a 1.6 mm radius Si_3N_4 ball, which correspond to an initial maximum Hertzian contact stress (P_{max}) of ~1.2 GPa. The sliding speed was fixed at 50 mm/s. The ratio of tangential to normal load is the friction coefficient. At least three POD tests were run out to a total sliding distance of 10 m (to show run-in friction behavior) or 140 m (to show steady-state friction behavior).

3. Results and discussion

Fig. 2 shows the X-ray diffraction (XRD) pattern for the as-deposited Ni–10Ti–10C composite. The primary peaks can be consistently indexed based on the face-centered cubic (FCC) Ni phase and the TiC phase exhibiting the rocksalt (NaCl-type) structure. A backscatter SEM image of this sample, shown in Fig. 3(a),

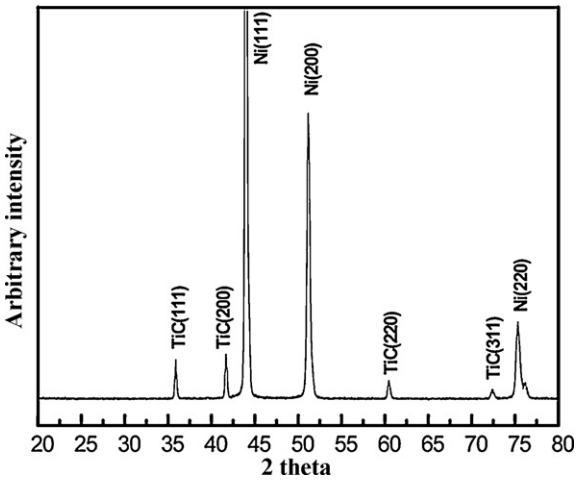

Fig. 2. XRD pattern obtained from the LENS deposited Ni–10Ti–10C sample.

clearly shows the presence carbides of two different morphologies and size scales. The coarser and faceted carbides are likely to be the primary TiC precipitates while the finer scale carbides are likely to be eutectic precipitates, homogeneously distributed within the Ni matrix. According to phase diagram of TiC–Ni system by Liu et al., it is eutectic reaction apparently at the Ni-rich corner consist of primary and eutectic TiC, which is consistent with current results [14].

Fig. 3(b)–(d) shows energy dispersive spectroscopy (EDS) maps of the exact same region as shown in Fig. 3(a), corresponding to different elemental species, Ti, Ni, and, C. Three of the EDS maps are at exactly the same magnification. These EDS maps clearly reveal that the primary carbide precipitates are enriched in Ti, depleted in Ni, and, enriched in C. High resolution Auger electron spectroscopy (AES) maps from a region of the Ni–10Ti–10C sample are shown in Fig. 4(b)–(d) with the corresponding SEM image shown in Fig. 4(a). The depletion of Ni (Fig. 4(b)), and the higher Ti (Fig. 4(c)) and C (Fig. 4(d)), within the carbide precipitates of both types is clearly visible. Based on Fig. 4(d), there appears to be some remnant C within the Ni matrix, which is unusual considering that solid Ni has negligible equilibrium solubility for C. However, the rapid solidification rates inherent during laser deposition via LENS might result in diffusion-limited trapping of C, resulting in some supersaturation within the Ni matrix. Bright-field transmission electron microscopy (TEM) images and electron diffraction patterns from these Ni–Ti–C composites are shown in Fig. 5. Fig. 5(a) shows the overall microstructure with both primary and eutectic carbide precipitates. Higher magnification bright-field images of the primary and eutectic carbides are shown in Fig. 5(b) and (c) respectively. Selected area electron diffraction patterns from these precipitates are shown as insets in both these figures. These diffraction patterns can be consistently indexed as the [0 0 1] and [1 1 2] zone axes of the TiC phase exhibiting a NaCl-type rocksalt structure. This is consistent with the result from the XRD pattern shown in Fig. 2. The primary TiC phase exhibits a relatively coarse-faceted structure, while the eutectic TiC exhibits fine grain structure having 200 nm size as shown in Fig. 5(d). It can be attributed to the increase of the hardness in this alloy.

A more detailed analysis of the Ni/TiC interface has been carried out using high-resolution TEM. Fig. 6(a) is a high-resolution TEM image showing relatively flat and planar carbide/nickel interface with the lattice planes visible in both phases. Fig. 6(b) shows a Fourier-filtered image of the interface, shown in Fig. 6(a), clearly exhibiting a 4-fold symmetry about the ⟨0 0 1⟩ axis (viewing direction) in the carbide region, and confirms that the titanium carbide exhibits a rocksalt structure. The corresponding viewing direction for the face-centered cubic (FCC) nickel phase in the same Fig. 6(b) is the 2-fold ⟨0 1 1⟩ FCC zone axis. The fast Fourier transform (FFT) image corresponding to Fig. 6(b) is shown in Fig. 6(c). Based on this FFT as well as other selected area electron diffraction patterns, the orientation relationship between the TiC and Ni phases was determined to be ⟨1 0 0⟩ TiC//⟨1 1 0⟩ FCC Ni and (0 0 2) TiC//($\bar{1}$ 1 1) Ni. The ($\bar{1}$ 1 1) interplanar spacing for FCC Ni is 2.0 Å and that of (0 0 2) planes in stoichiometric TiC is 2.2 Å, with a misfit of 10%. The carbide/nickel interface plane appears to be oriented at an angle of 20° from the (1 $\bar{1}$ 1) planes of FCC Ni and at an angle of 30° from

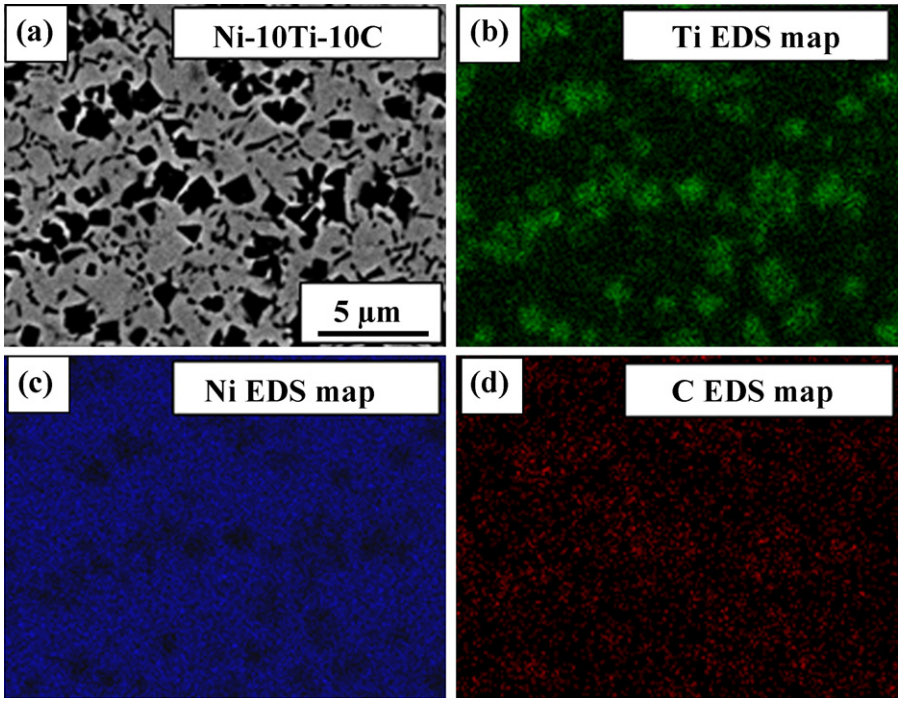

Fig. 3. Backscatter SEM image and EDS maps of LENS deposited of Ni–10Ti–10C sample.

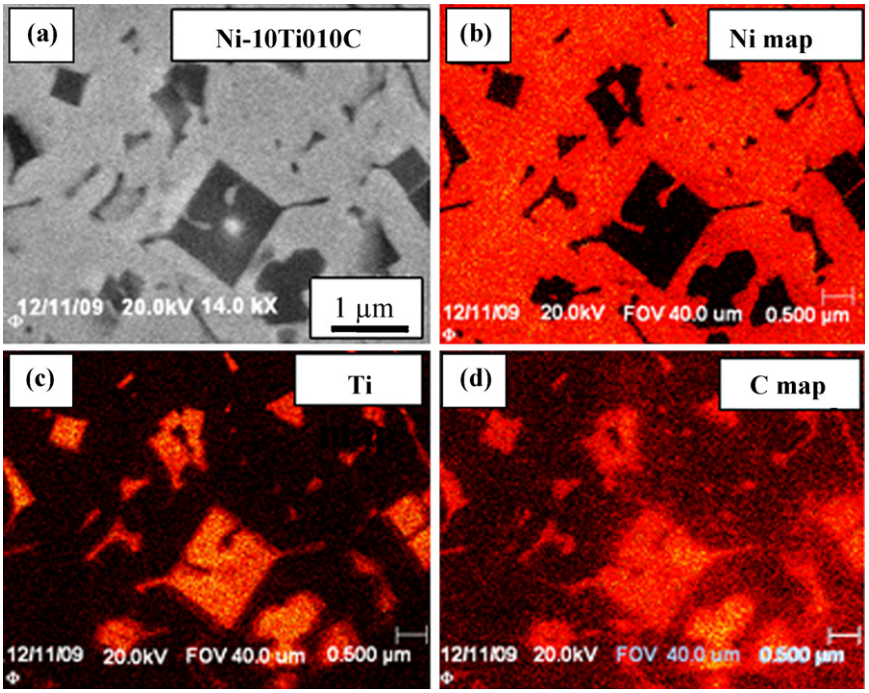

Fig. 4. SEM image (a) and corresponding Auger electron spectroscopy maps (512 × 512 pixels) of (b) Ni, (c) Ti, and (d) C. The thermal pseudocolor images show relative amounts of the constituents.

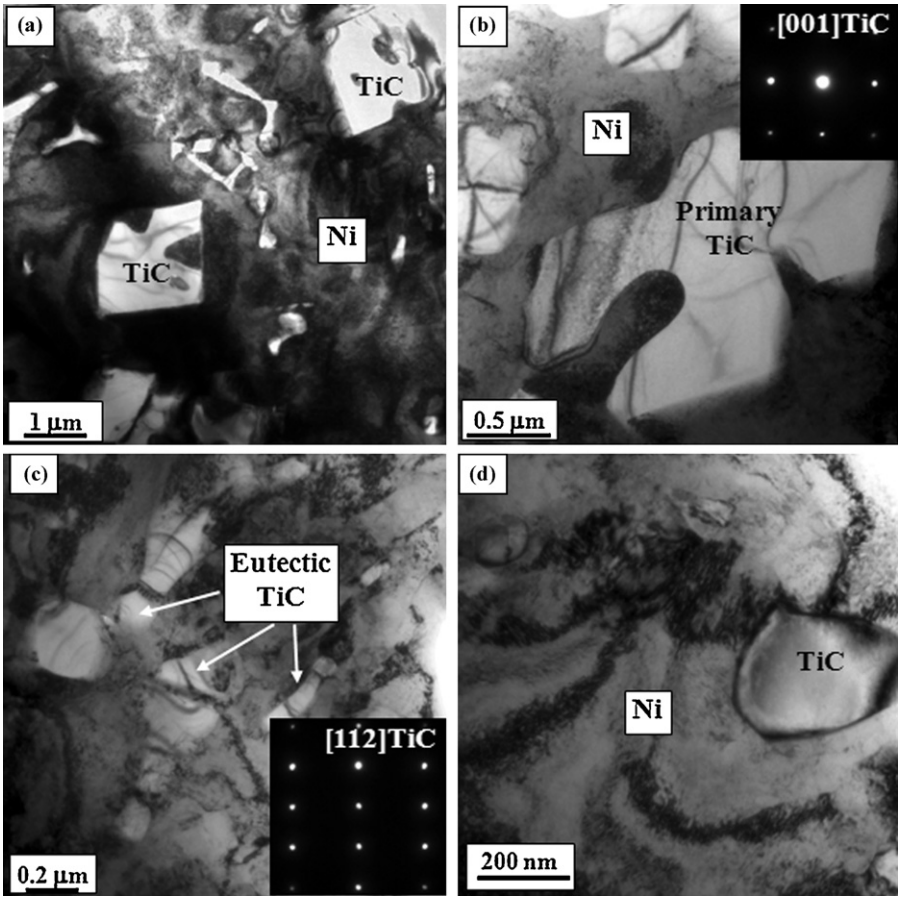

Fig. 5. Bright-field TEM image showing the TiC phase (a), higher magnification image showing primary TiC phase with SAD pattern in an inset (b), higher magnification of eutectic TiC phase with SAD pattern in an inset (c), and (d).

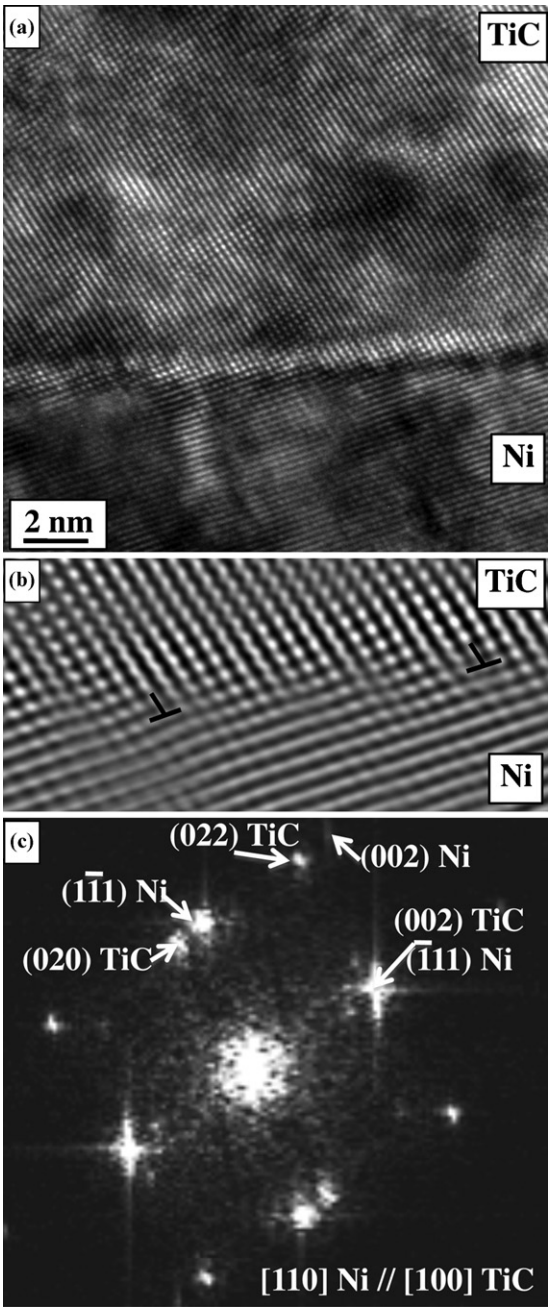

Fig. 6. HRTEM image showing interface between Ni matrix and TiC (a), and higher magnification image showing semi-coherent interface after filtering of HRTEM image, and (c) FFT spectra showing specific orientation relationship.

the (0 2 0) planes of TiC. Based on this analysis, the interface plane appears to be parallel to the (1 $\bar{1}$ 2) planes of FCC Ni. Theoretically the angle between (1 $\bar{1}$ 2) and (1 $\bar{1}$ 1) of Ni should be 19.4° that is in close agreement with the experimentally measured value. Additionally, the FCC Ni phase being substantially softer (lower elastic constants) as compared with the TiC phase, results in the partitioning of the elastic strain arising from the misfit between the two phases more towards the FCC Ni phase. Consequently the FCC Ni matrix has a high degree of strain as clearly visible in Fig. 6(b). Furthermore, the strain at carbide/nickel interface, arising from the misfit between the two phases, is partially relieved by the formation of misfit dislocations at the interface, shown in the magnified view of the interface in Fig. 6(b), separating coherent regions of excellent lattice matching. The sequence of phase formation for this composite is: Ni–10Ti–10C: liquid Ni (Ti,C) → liquid Ni + primary TiC → primary TiC + eutectic (Ni + TiC).

The Ni–10Ti–10C composite exhibited a high microhardness value of 370 VHN in comparison to 165 VHN for LENS deposited pure Ni. The high volume fraction of titanium carbides (both primary and eutectic) resulted in this higher microhardness value. Preliminary results of the POD tribometry studies carried out on the LENS deposited Ni–10Ti–10C composite and pure Ni sample are shown in Fig. 7. The samples were tested to either a total sliding distance of 10 m, Fig. 7(a), or 140 m, Fig. 7(b). These distances allow for a comparison between run-in (early stage) friction behavior and steady-state friction behavior, respectively. From Fig. 7, it is clear that the TiC phases in the composite were beneficial in reducing the friction coefficient during the entire run-in and steady-state regimes with respect to the pure Ni sample. Therefore, this friction coefficient reduction of ~0.2 during run-in and ~0.25 during steady-state can be attributed to the presence of primary and eutectic TiC. The reason for the initial transition from low to high friction coefficient during the run-in regime, shown in Fig. 7(a), may be a result of the removal of the nascent oxide film on the surface of the composite. Meanwhile, the longer run-in period, shown in Fig. 7(b) before steady-state friction coefficients of ~0.5 and 0.75 are achieved, may be due to the increase in plowing (abrasive) component of friction because of metallic roughen-

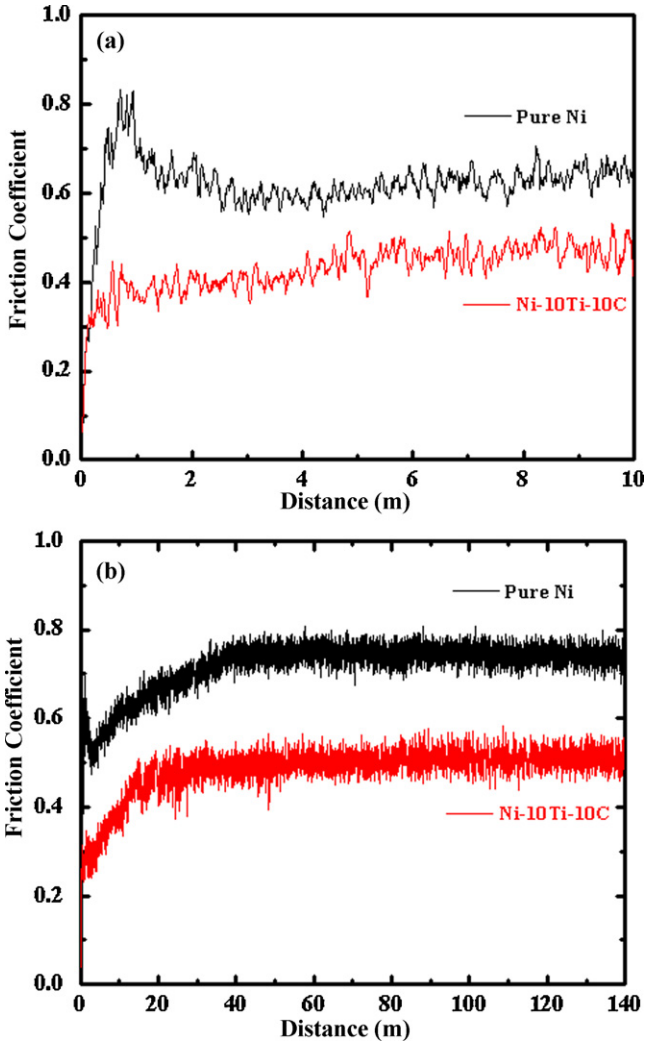

Fig. 7. Run-in and steady-state friction coefficients as a function of sliding distance up to 10 m (a) and 140 m (b), respectively, for LENS deposited Ni–10Ti–10C composite and pure Ni.

ing in the sliding contact. However, more detailed studies of the structural and chemical modifications inside the wear tracks are currently underway to explain these friction coefficient transitions. While the steady-state friction coefficient for the LENS deposited Ni–10Ti–10C composite is only ~0.1 higher than that of previously reported self-lubricating LENS deposited Ni/multi-walled carbon nanotube (MWCNT) composite [16], its microhardness is much higher by ~100 VHN. Thus, the Ni–10Ti–10C composite appears to be a promising material for surface engineering applications requiring high hardness with improved solid lubrication.

4. Conclusions

In situ composite of nominal composition Ni–10Ti–10C has been deposited using the laser engineered net shaping (LENS) process. The as-deposited microstructure exhibits a large volume fraction of primary faceted TiC precipitates distributed within a eutectic Ni + TiC matrix. The TiC precipitates exhibit the rocksalt structure with the orientation relationship between the TiC and FCC Ni phases being $\langle 1\,0\,0\rangle$ TiC//$\langle 1\,1\,0\rangle$ FCC Ni and $(0\,0\,2)$ TiC//$(\bar{1}\,1\,1)$ FCC Ni. The Ni/TiC interface appears to be semi-coherent with misfit dislocations separating the regions of coherency between the two phases. Preliminary tribological and mechanical property measurements reveal the steady-state friction coefficient for this composite to be ~0.5, lower than pure Ni, and with a substantially higher hardness, making this a promising candidate for surface engineering applications that require both solid lubrication and high mechanical hardness.

Acknowledgements

This work was financially supported by the U.S. Air Force Research Laboratory (AFRL, ISES Contract No. FA8650-08-C-5226). The authors also gratefully acknowledge the Center for Advanced Research and Technology (CART) at the University of North Texas. Two of the authors (B.A.M. and T.W.S.) acknowledge the partial support of the National Science Foundation (Grant No. CMMI-0700828).

References

[1] D.B. Miracle, Compos. Sci. Technol. 65 (2005) 2526–2540.
[2] S.C. Tjong, Z.Y. Ma, Mater. Sci. Eng. R 29 (2000) 49–113.
[3] W. Liu, J.N. Dupont, Metall. Mater. Trans. A 35 (2004) 1133–1140.
[4] D. Strzeciwilk, Z. Wokulski, P. Tkacz, J. Alloys Compd. 350 (2003) 256–263.
[5] D.E. Burkes, J.J. Moore, J. Alloys Compd. 430 (2007) 274–281.
[6] B. Zheng, T. Topping, J.E. Smugeresky, Y. Zhou, A. Biswas, D. Baker, E.J. Lavernia, Metall. Mater. Trans. A 41 (2010) 568–573.
[7] Y. Du, J.C. Schuster, Z. Metallkd. 89 (1998) 399–410.
[8] J.Y. Huang, L.L. Ye, Y.K. Wu, H.Q. Ye, Acta Mater. 44 (1996) 1781–1792.
[9] Y.F. Yang, H.Y. Wang, J.G. Wang, R.Y. Zhao, Q.C. Jiang, J. Alloys Compd. 486 (2009) 191–194.
[10] B.C. Langelier, S. Esmaeili, J. Alloys Compd. 482 (2009) 246–252.
[11] D. Liu, S.Q. Zhang, A. Li, H.M. Wang, J. Alloys Compd. 485 (2009) 156–162.
[12] D. Liu, S.Q. Zhang, A. Li, H.M. Wang, J. Alloys Compd. 496 (2010) 189–195.
[13] Y. Li, P. Bai, Y. Wang, J. Hu, Z. Guo, Mater. Design. 30 (2009) 1409–1412.
[14] Z.D. Liu, J. Tian, B. Li, L.P. Zhao, Mater. Sci. Eng. A 527 (2010) 3898–3903.
[15] C. Atwood, M. Griffith, L. Harwell, E. Schlienger, M. Ensz, J. Smugeresky, T. Romero, D. Greene, D. Reckaway, Proceedings of the Laser Material Processing Conference (ICALEO'98), Orlando, FL, USA, 1998, pp. E1–E7.
[16] T.W. Scharf, A. Neira, J.Y. Hwang, J. Tiley, R. Banerjee, J. Appl. Phys. 106 (013508) (2009) 1–7.
[17] X. Wu, J. Mei, J. Mater. Process. Tech. 135 (2003) 266–270.